



# A hybrid approach for cutting force prediction in flank milling based on analytical and 3D finite element method

Junli Li<sup>1</sup> · Xiaojiang Cai<sup>2</sup> · Qinglong An<sup>3</sup> · Ming Chen<sup>3</sup>

Received: 26 February 2020 / Accepted: 5 August 2020 / Published online: 25 August 2020  
© Springer-Verlag London Ltd., part of Springer Nature 2020

## Abstract

Flank milling is one of the most widely used milling processes characterized by high machining efficiency. However, due to the low thermal conductivity and high-temperature strength of nickel-based superalloy Inconel 718, flank milling of Inconel 718 is still an extremely difficult and challenging task in which the milling cutter suffers large cutting force and excessive tool wear. Therefore, prediction of cutting force in milling process has caused due attention and became a major concern in manufacturing process. The present work is thus aimed at developing a new cutting force model for flank milling, which might try to eliminate the drawbacks of pure analytical force model, data-based reasoning method (DBRM), and full three dimensional (3D) finite elements (FE) model. The hybrid cutting force model is conducted by discretizing cutting edge into fragments based on infinitesimal method and regarding each fragment as a 3D oblique cutting FEM model. With the integration of 3D predicted cutting force along the axis considering the run-in and run-out effect of each cutting edge, the predicted cutting force can be obtained. Finally, the predicted results showed a good agreement with that of experimental.

**Keywords** Flank milling · Cutting force prediction · Hybrid model · Finite difference method · 3D finite element

## Abbreviations

FE	Finite element	$\dot{\varepsilon}_0$	Strain rate parameter
$F_{aj}$	Cutting force in axial direction	$\dot{\varepsilon}^{pl}$	Equivalent plastic strain rate
$F_{rj}$	Cutting force in radial direction	$\bar{\varepsilon}_f^{pl}$	Equivalent failure plastic strain
$F_{tj}$	Cutting force in tangential direction	$\varepsilon^{el}$	Elastic strain
$\alpha_n$	Tool normal rake angle	$\varepsilon^{th}$	Strain caused by heat extension
$\eta_c$	Chip-flow angle	$v_c$	Cutting speed
$i$	Inclination of the main cutting edge	$v_f$	Feed rate (mm/min)
$f_z$	Feed per tooth (mm/tooth)	$\alpha_e$	Tool effective rake angle
$D$	Diameter of the milling cutter (mm)	$\theta_j$	Position angle of cutter
$h$	Equivalent undeformed chip height	$T_0$	Reference temperature
$l'$	Equivalent undeformed chip length	$T_m$	Melting temperature
$\sigma$	Flow stress	$A$	JC material parameters
$\varepsilon^{pl}$	Equivalent plastic strain	$B$	JC material parameters
		$C$	JC material parameters
		$n$	JC material parameters
		$m$	JC material parameters
		$\tau_f$	Frictional stress
		$\sigma_n$	Normal stress
		$\psi$	Phase difference
		$\sigma_s$	Shear flow stress
		$T$	Temperature parameter
		$a_p$	Axis depth of cut
		$d_1 \sim d_5$	Failure parameters

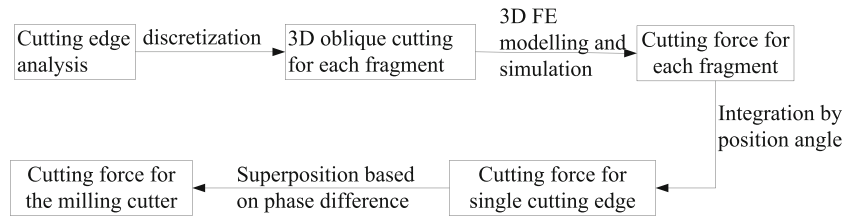
✉ Junli Li  
junl@sues.edu.cn

<sup>1</sup> School of Mechanical Engineering, Shanghai University of Engineering Science, Shanghai 201620, People's Republic of China

<sup>2</sup> Shanghai Aerospace Control Technology Institute, Shanghai 201109, People's Republic of China

<sup>3</sup> School of Mechanical Engineering, Shanghai Jiao Tong University, Shanghai 200240, People's Republic of China

**Fig. 1** Schematic of milling force modeling



### 1 Introduction

Nickel-based superalloy Inconel 718 has been broadly applied in the field of aerospace, automotive, energy, and biomedical industries due to its superior properties. These properties are its wear resistance, high melting temperature, high corrosion and creep resistance, and maintaining strength and hardness at high temperatures. Despite the aforementioned superior properties, the machinability of Inconel 718 continues to pose a challenge owing to factors including high temperatures, large cutting force, strong work hardening, and inefficient chip fracturing behavior. These undesirable parameters cause to higher mechanical loads, and high cutting temperatures at the chip-tool interface result in increased tool wear, reduced productivity, reduced process reliability, and increased surface roughness [1].

Flank milling is one of the most widely used milling processes characterized by high machining efficiency. However, despite its high machining efficiency, flank milling of Inconel 718 is still an extremely difficult and challenging task due to large cutting force and excessive tool wear. Therefore, predicting cutting force in milling process has caused due attention and became a major concern in manufacturing sectors. Superior cutting force prediction model typically can

attain the results of reduced machining cost, improved surface quality, and expanded tool life.

Analytical model based on mechanical mechanism has been widely used in cutting force prediction for its inherent advantages with considering the machining process such as uncut chip thickness variation, tool run-out effect, tool vibration, and elastic recovery. Based on this, analytical model was especially employed in the cutting force prediction for micro-end milling with a special focus on size effect. Wojciechowski et al. [2] focused on the prediction of cutting forces during micro-end milling using a novel approach that takes into account the chip thickness accumulation phenomenon. Zhang et al. [3] proposed a milling force model for micro-end milling based on size effect of specific cutting force. The milling edges were divided into many elements, and every element was regarded as an orthogonal cutting process in their model. Srinivasa et al. [4] proposed a mechanistic model to predict the cutting forces in micro-end milling operation taking into account overlapping tooth engagements. Results showed that the mechanistic model predicts the transverse force with an average absolute error of 12.29%, while a higher prediction error of 19.49% is obtained for feed force. Harry et al. [5] presented analytical models with calculating the instantaneous uncut chip geometry for orthogonal centric turning-milling

**Fig. 2** Schematic of tiny element method of milling process

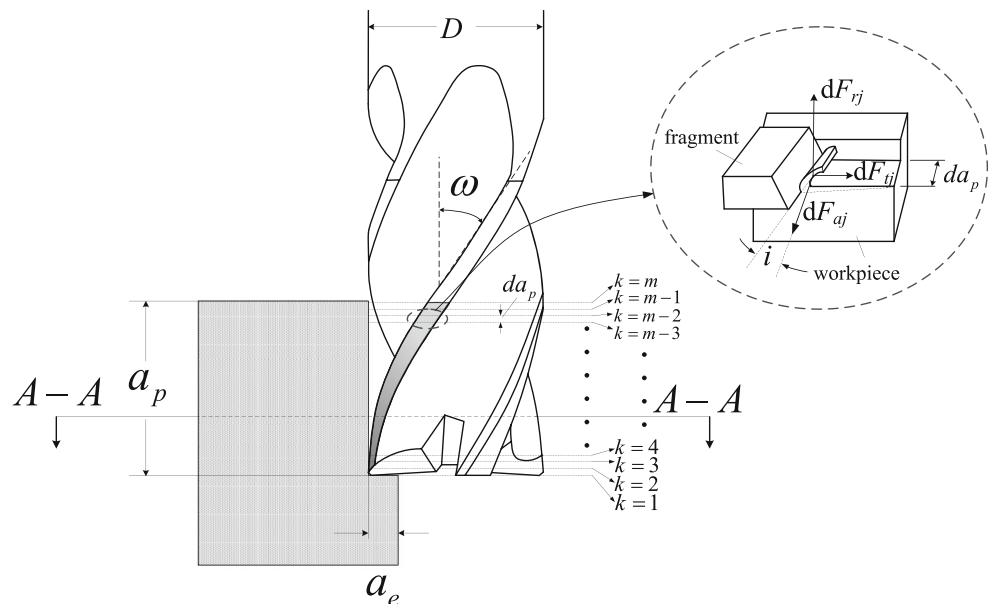
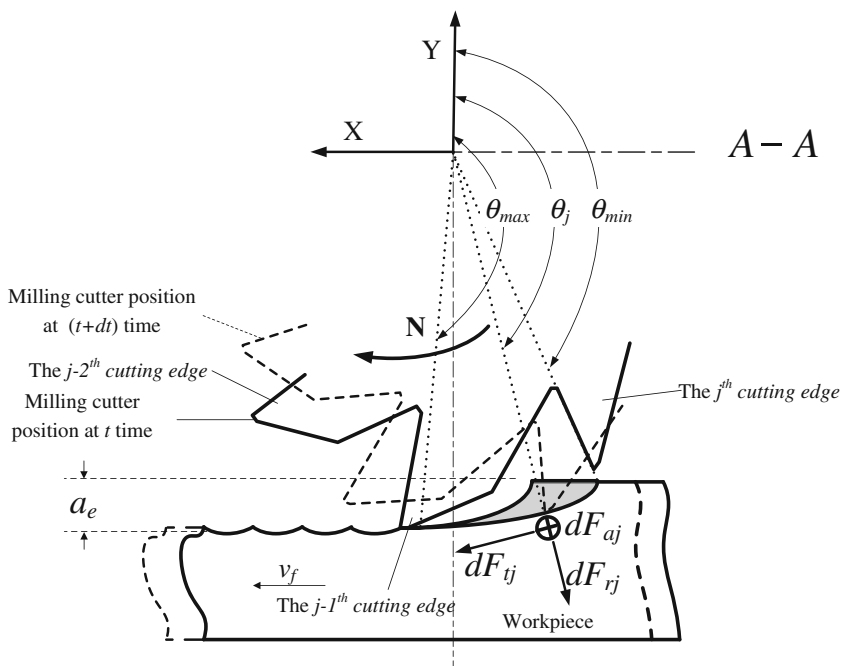


**Fig. 3** Geometric schematic of milling process



operations to predict cutting force. Ma et al. [6] presented calculation methods of uncut chip thickness and cutting tool swept area for curved surface in the ball-end milling process. Wan et al. [7] developed a new ternary-mechanism cutting force model including chip removal, flank rubbing, and bottom cutting effects to predict cutting forces in flat-end milling. Wei et al. [8] presented a cutting force coefficient identification model related to chip thickness and axial position angle. Results showed that the milling force coefficients and run-out parameters can be applied to fillet end milling under predetermined inclination angle well. Wang et al. [9] proposed a cutting force prediction model in 5-axis milling considering cutter run-out and vibrations. The influence of cutter run-out

and cutter vibrations are modeled as extra terms on the designed uncut chip thickness. Guo et al. [10] presented a cutting force coefficient identification model, which is related to the instantaneous chip layer thickness and axial position angle considering the cutter run-out. Berglind et al. [11] developed a discretization approach to predict cutting force in 5-axis milling, in which the tool is composed of multiple cutting elements. Su et al. [12] applied a dynamic contact model to predict milling force for a complex profile milling cutter. The cutting edge is discretized into a number of fragments along its axis based on infinitesimal method. Tuysuz et al. [13] concluded that the identification of tool indentation zone and the modeling of its contact mechanics greatly improve the

**Fig. 4** Schematic of 3D finite element modeling for fragment

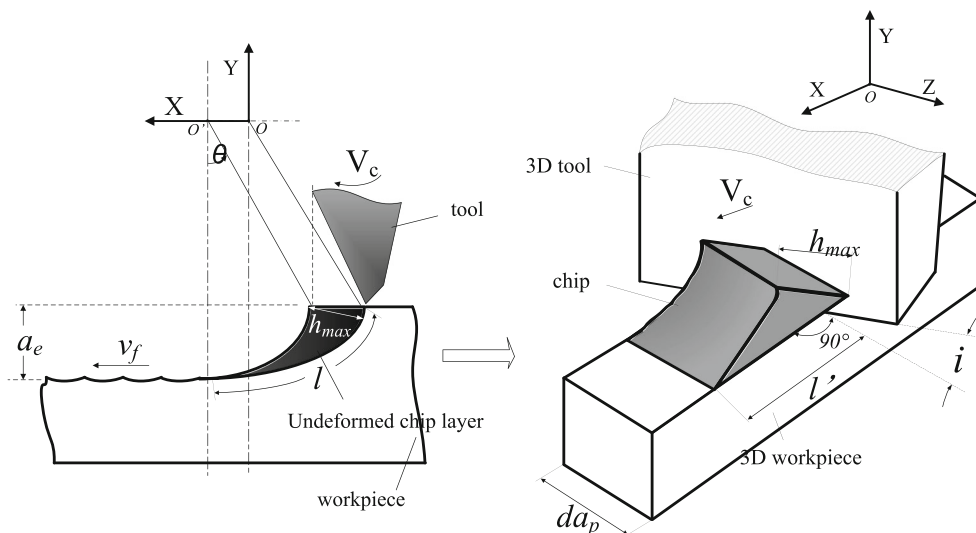


**Table 1** Value of parameters in fragment modeling ( $a_e = 0.2$  mm)

$da_p$ (mm)	0.1	$m$	100
$h_c$ (mm)	0.05, 0.1, 0.15	$\Psi$ (°)	29.66
$l'$ (mm)	1.524 ( $f_z = 0.05$ ), 1.499 ( $f_z = 0.1$ ), 1.474 ( $f_z = 0.15$ )	$\theta_{\min}$ (°)	165.17
$\theta_{\max}$ (°)	180.48, 180.96, 181.44	$v_c$ (m/min)	20, 50, 80, 110

prediction of axial ( $z$ ) cutting forces in ball-end milling. Wojciechowski [14] predicted milling forces of micro-ball end on the basis of mechanistic model considering run out, variable edge forces, and kinematics of low radial immersion milling with tool axis inclination.

However, despite its excellent property and prospective applications, analytical model has its own drawbacks involved in complicated establishment of model and time-consuming, which extremely depends on the capability of engineers and shrinks the application in actual machining process. Therefore, data-based reasoning method (DBRM) such as adaptive network-based fuzzy inference system and neural network, regression method, and finite element method (FEM) were developed for cutting force predictions during milling process. Thellaputta et al. [15] stated that the prediction capability of DBRM model is more accurate than the regression model for milling force prediction. Empirical uncertain components of cutting forces considering tool wear have been established by using a radial basis function neural network [16]. Aristimuno et al. [17] improved cutting force predictions when milling martensitic stainless using an optimization methodology for material databases. The predictions showed an improvement compared with those of the strategy of keeping constant the specific edge coefficient. Jamal et al. [18] utilized the mechanistic modeling approach in combination with neural networks data fitting for simulating the cutting forces in the milling of unidirectional carbon fiber reinforced polymers.

FEM has been used to model cutting process for its excellent performance in chip formation, strain and stress distribution, temperature, and cutting force prediction. Sahoo et al. [19] adopted a hybrid approach with the aggregation of both FEM simulation and mechanistic approach with consideration of modified undeformed chip thickness algorithm for prediction of cutting forces in micro-end milling. Cai et al. [20] proposed a novel cutting force prediction model based on non-uniform rational basis splines and FE method. The cutting force prediction method has a similar accuracy with the method of coefficient identification and is more efficient than the

FE method. Time domain simulation containing both the tool and workpiece dynamics in two directions and a mechanistic force model were used to numerically estimate the cutting forces in milling of flexible workpieces [21]. Ducobu et al. [22] introduced a 3D finite element coupled Eulerian-Lagrangian model of orthogonal cutting that faithfully reproduces the experimental operation and is verified by comparison with it. Nasr and Ammar [23] compared two damage modeling approaches in metal cutting finite element simulations. Results showed that considered damage evolution were more successful in predicting cutting forces, shear angle, chip thickness, and contact length. Pratap et al. [24] presented a FEM-based micro-end milling cutting force modeling of Ti-6Al-4V titanium alloy microchannels. The finite element simulation of specific cutting forces showed the size effects in micro-end milling process. Jing et al. [25] presented a cutting force model for the micro-end-milling processes using a hybrid approach based on FEM and cutting force coefficients. The cutting force coefficients are extracted through a nonlinear algorithm to establish a relationship with the uncut chip thickness and cutting speed.

In spite of various studies concerning on cutting force predictions during milling process, researches regarding the effect of tool run-in and run-out, the combination of analytical method, and FEM involved in cutting force prediction are very limit and rare found in flank milling. Since analytical model exhibits a complicate established and calculation process, while large experimental databases are required for DBRM model as well as the inherent contradiction between the accuracy and efficiency in the pure FEM, accurate and efficient cutting force prediction in flank milling seems to become a key concern.

By taking into consideration of the existing scope, the current study proposes a modified hybrid approach for cutting force prediction in flank milling. Specially, the cutting edge is discretized into a number of fragments along its axis based on infinitesimal method and each fragment is regard as a 3D oblique cutting process modeled by FEM. The cutting force can be gained by integrating the predicted cutting force of fragments along the axis considering the cutting-in and cutting-out effect of each cutting edge. The main object of the present paper is to provide an accuracy and efficiency cutting force prediction model for flank milling, which is helpful in selecting milling parameters, designing milling cutters, and choosing milling methods.

**Table 2**  $J$ - $C$  parameters for Inconel 718 alloy [27]

$A$ (MPa)	$B$ (MPa)	$N$	$C$	$\varepsilon_0$	$m$
1241	622	0.6522	0.0134	1	1.3

**Table 3** Physical properties of Inconel 718, Haglund et al. [28]

Material properties	Inconel 718
Poisson's ratio	0.3
Density (kg/m <sup>3</sup> )	8190
Young's modulus (GPa)	201(20 °C), 192(200 °C), 185 (400 °C), 173(600 °C), 154(800 °C)
Specific heat (J/kg °C)	451(20 °C), 482(200 °C), 494(400 °C), 539 (600 °C) 615 (800 °C), 707 (900 °C)
Thermal conductivity (W/m °C)	13.4 (20 °C), 15.9 (200 °C), 18.3 (400 °C), 21.2(600 °C)23.6(800 °C), 30.4(900 °C)
Coefficient of linear thermal expansion (mm/mm °C)	13.1 × 10 <sup>-6</sup> (20 °C), 13.8 × 10 <sup>-6</sup> (200 °C), 14.7 × 10 <sup>-6</sup> (400 °C), 15.3 × 10 <sup>-6</sup> (600 °C), 17.1 × 10 <sup>-6</sup> (600 °C)

## 2 Basic mechanistic model for flank milling

Based on the aforesaid analysis, cutting forces have been predicted by the proposed hybrid model, which has been presented through a flow chart as shown in Fig. 1. The flow chart clearly reveals the hybridization of the model by incorporating the analytical model and FEM simulation.

Further, 3D oblique cutting FE model was used to predict cutting force for fragments discretized from the cutting edge by infinitesimal method. Cutting force of each cutting edge could be obtained with the integration of predicted fragment cutting force based on position angle. Finally, the cutting force of the milling cutter could be conducted by the superposition of cutting edge phase difference involved in cutting process. Attributed to the mechanical-based establishment of cutting force model, as well as the utilizing of 3D oblique FE cutting model for fragment, the proposed hybrid model seems to be able to predict cutting force more convenient and efficiency compared with the pure analytical, DBRM, and complete 3D milling FE model.

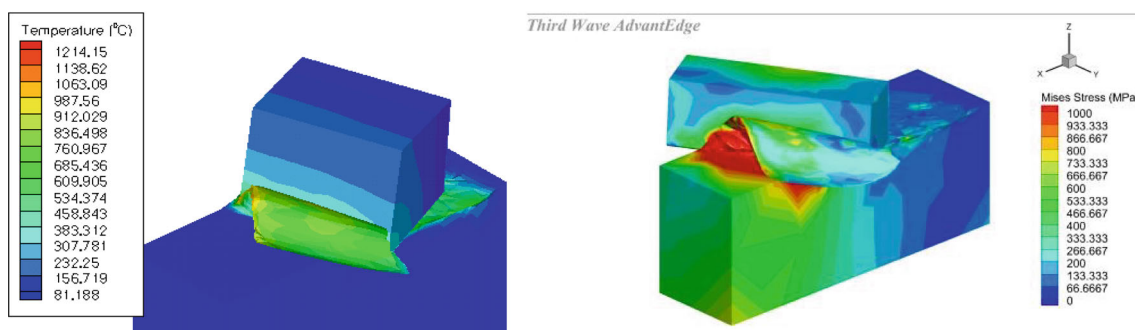
## 3 Cutting force model based on finite difference method

The basic idea of finite difference method is to replace the solution of partial differential equation with interpolation

polynomial and its differential. Its basic steps include region discretization, approximate substitution, and approximate solution. Thereby, it can be conducted that this method is very suitable for modeling the cutting force of milling cutter with helix angle. Taking the end mill in this paper as an example, a certain number of cutting edges (four in the current work) are evenly distributed on the cylindrical surface. Adjacent cutting edges participate in cutting along the rotation direction of the milling cutter with a fixed phase difference. The number of cutting edges participating in cutting at any time is determined by the radial depth of cut and the number of teeth of milling cutter.

Figure 2 depicts the schematic diagram of a 3D oblique cutting micro-element modeling based on variable thickness, and Fig. 3 exhibits the schematic diagram of a geometric relationship of a milling process. Assuming that the  $j$ th cutting edge was discretized into the same fragment with the number of  $m$ , thus, each fragment could be regard as oblique cutting process with an inclination angle  $i$ , thereby 3D oblique FE cutting model could be established for each fragment and then the cutting forces of these fragments  $dF_{aj}$ ,  $dF_{rj}$ , and  $ddF_{ij}$  could be acquired. Based on this, the integral cutting force of the milling cutter could be obtained with the integration of fragment cutting force by mathematic software MATLAB.

With reference to the position of the fragment at the bottom of the  $j$ th cutting edge (first participating in the cutting process along with the rotation of the milling cutter), the position angle

**Fig. 5** 3D finite element modeling of oblique cutting



**Table 4** Chemical composition of Inconel 718, wt%

C	Cr	Ni	Co	Mo	Nb	Al	Ti	Fe
≤ 0.08	17.0~21.0	50.0~55.0	≤ 1.0	2.80~3.30	4.75~5.5	0.30~0.70	0.75~1.15	Other

at a certain time in the cutting process is set as  $\theta_j$ , the angle for cutting into the workpiece material is  $\theta_{\min}$ , and the corresponding run-out angle is  $\theta_{\max}$ . At this time, the fragment of cutting edge undergone the complete process for cutting thickness reduced from maximum to 0, as shown in Fig. 3.

Through the preceding analysis it could be clear that the cutting force  $dF_{aj}$ ,  $dF_{rj}$ , and  $dF_{tj}$  has the functional relationship with the position angle  $\theta_j$ , which could be expressed as  $dF_{aj}(\theta_j)$ ,  $dF_{rj}(\theta_j)$ , and  $dF_{tj}(\theta_j)$ , respectively. Thereby, the three-dimensional forces of the fragment, i.e., tangential force  $dF_{tj}(\theta_j)$ , radial force  $dF_{rj}(\theta_j)$ , and axial force  $dF_{aj}(\theta_j)$ , can be transformed into the cutting force measured by the force measuring instrument in the coordinate system of the machine tool through the geometric relationship, as shown in Eq. (1).

$$\begin{pmatrix} dF_{xj}(\theta_j) \\ dF_{yj}(\theta_j) \\ dF_{zj}(\theta_j) \end{pmatrix} = \begin{bmatrix} -\cos\theta_j & -\sin\theta_j & 0 \\ -\sin\theta_j & \cos\theta_j & 0 \\ 0 & 0 & 1 \end{bmatrix} \begin{pmatrix} dF_{tj}(\theta_j) \\ dF_{rj}(\theta_j) \\ dF_{aj}(\theta_j) \end{pmatrix} \quad (1)$$

The cutting force of the  $j$ th cutting edge in the coordinate system of the machine tool can be obtained by sequentially accumulating the three-dimensional cutting forces of all the fragments involved in cutting on the  $j$ th cutting edge in turn with a certain phase difference, as shown follows:

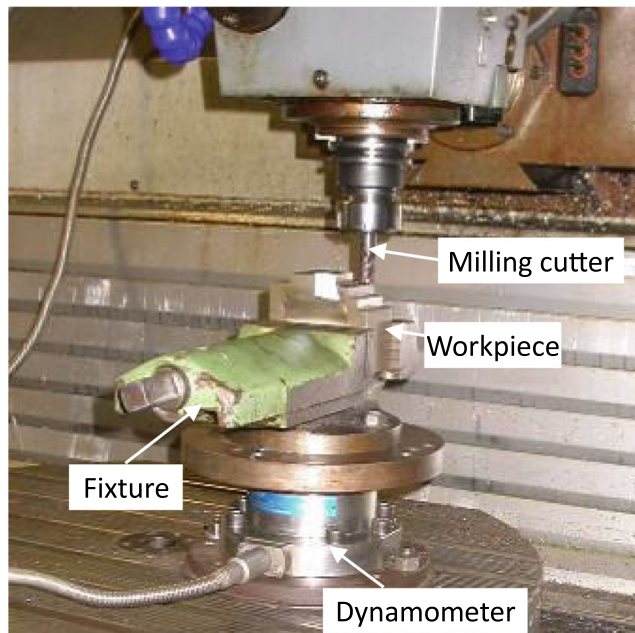


**Fig. 6** Experimental setup

$$\begin{aligned} F_{xj}(\theta_j) &= \sum_{k=m_{\min}}^{m_{\max}} [-F_{tj}(\theta_{jk}) \cdot \cos\theta_{jk} - F_{rj}(\theta_{jk}) \cdot \sin\theta_{jk}] \\ F_{yj}(\theta_j) &= \sum_{k=m_{\min}}^{m_{\max}} [-F_{tj}(\theta_{jk}) \cdot \sin\theta_{jk} + F_{rj}(\theta_{jk}) \cdot \cos\theta_{jk}] \\ F_{zj}(\theta_j) &= \sum_{k=m_{\min}}^{m_{\max}} F_{aj}(\theta_{jk}) \end{aligned} \quad (2)$$

where  $m_{\min}$  and  $m_{\max}$  are the upper and lower limits of the number of fragment involved in cutting process on the  $j$ th cutting edge and  $\theta_{jk}$  is the position angle of the  $k$ th fragment on the  $j$ th cutting edge, which can be obtained as follow:

$$\theta_{jk} = \theta_j - \frac{\psi(k-1)}{m} \quad (3)$$

where  $\psi$  is the maximum phase difference of a single cutting edge participating in the cutting process, which is the phase difference between the fragment  $k = 1$  and the fragment of  $k = m$ , as shown follow:

$$\psi = 2a_p \operatorname{tg} i / D \quad (4)$$

Obviously, due to the existence of the helix angle, the  $m$  fragments on the  $j$ th edge do not participate in the cutting at the same time, but gradually cutting-in and cutting-out of the workpiece material with a certain phase difference. The number of fragments participating in the cutting process at the same time is between 1 and  $m$ , which can be divided into the following situations:

(1)  $\theta_{\max} - \theta_{\min} \geq \psi$

**Table 5** Design of milling tests

No.	Factors	
	$v_c$ (m/min)	$f_z$ (mm/z)
1	30	0.05
2	30	0.10
3	30	0.15
4	70	0.05
5	70	0.10
6	70	0.15
7	110	0.05
8	110	0.10
9	110	0.15

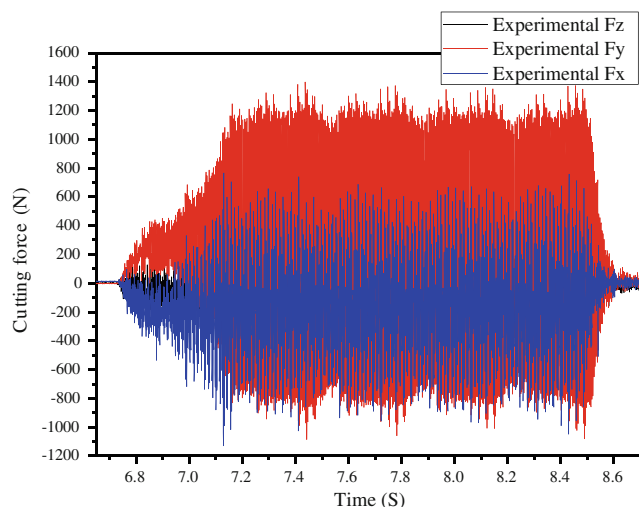


Fig. 7 Experimental cutting force for test 5

In this case, the entire cutting edge has a period of participation in the cutting process in the range of the axial depth of cut. The upper and lower limits are determined according to the three positions of the position angle:

$$\begin{aligned}
 \theta_j \in [\theta_{\min}, \theta_{\min} + \psi] &\rightarrow m_{\min} = 1; m_{\max} = \left[ m \cdot \frac{\theta_j - \theta_{\min}}{\psi} \right]^* \\
 \theta_j \in (\theta_{\min} + \psi, \theta_{\max}] &\rightarrow m_{\min} = 1; m_{\max} = m \\
 \theta_j \in (\theta_{\max}, \theta_{\max} + \psi] &\rightarrow m_{\min} = \left[ \frac{\theta_j - \theta_{\max}}{\psi} \cdot m \right]^*; m_{\max} = m
 \end{aligned} \tag{5}$$

(2)  $\theta_{\max} - \theta_{\min} < \psi$

In this case, the  $m$ th fragment in the uppermost on the edge line has not yet entered the cutting area, and the first fragment in the lowermost has left the cutting area. The upper and lower limits are also determined according to the three positions of the position angle  $\theta_j$ :

$$\begin{aligned}
 \theta_j \in [\theta_{\min}, \theta_{\max}] &\rightarrow m_{\min} = 1; m_{\max} = \left[ m \cdot \frac{\theta_j - \theta_{\min}}{\psi} \right]^* \\
 \theta_j \in (\theta_{\max}, \theta_{\min} + \psi] &\rightarrow m_{\min} = \left[ m \cdot \frac{\theta_j - \theta_{\max}}{\psi} \right]^*; m_{\max} = \left[ m \cdot \frac{\theta_j - \theta_{\min}}{\psi} \right]^* \\
 \theta_j \in (\theta_{\min} + \psi, \theta_{\max} + \psi] &\rightarrow m_{\min} = \left[ \frac{\theta_j - \theta_{\max}}{\psi} \cdot m \right]^*; m_{\max} = m
 \end{aligned} \tag{6}$$

where the square brackets marked with asterisk are rounded, since the cutting edges are discretized and numbered, the upper and lower limits  $m_{\min}$  and  $m_{\max}$  should be natural numbers within the range of 1 to  $m$ . After determining the upper and lower limits of the integration, the cutting force of single edge can be

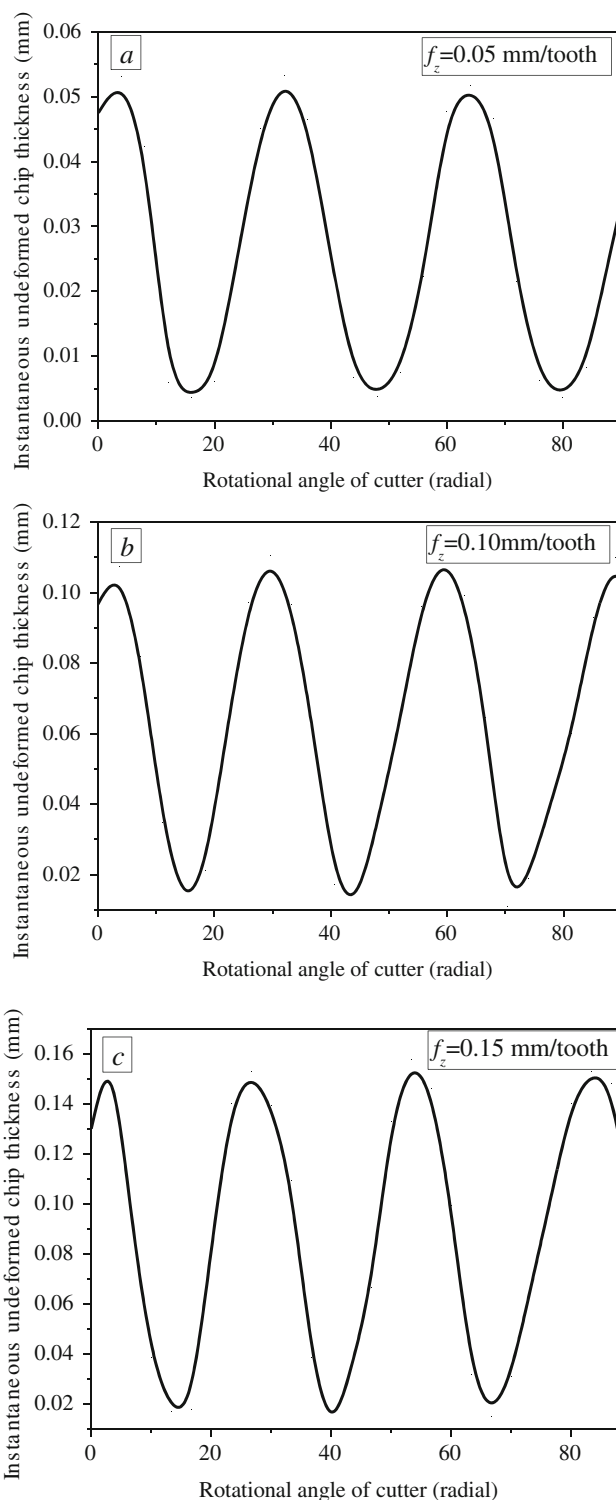
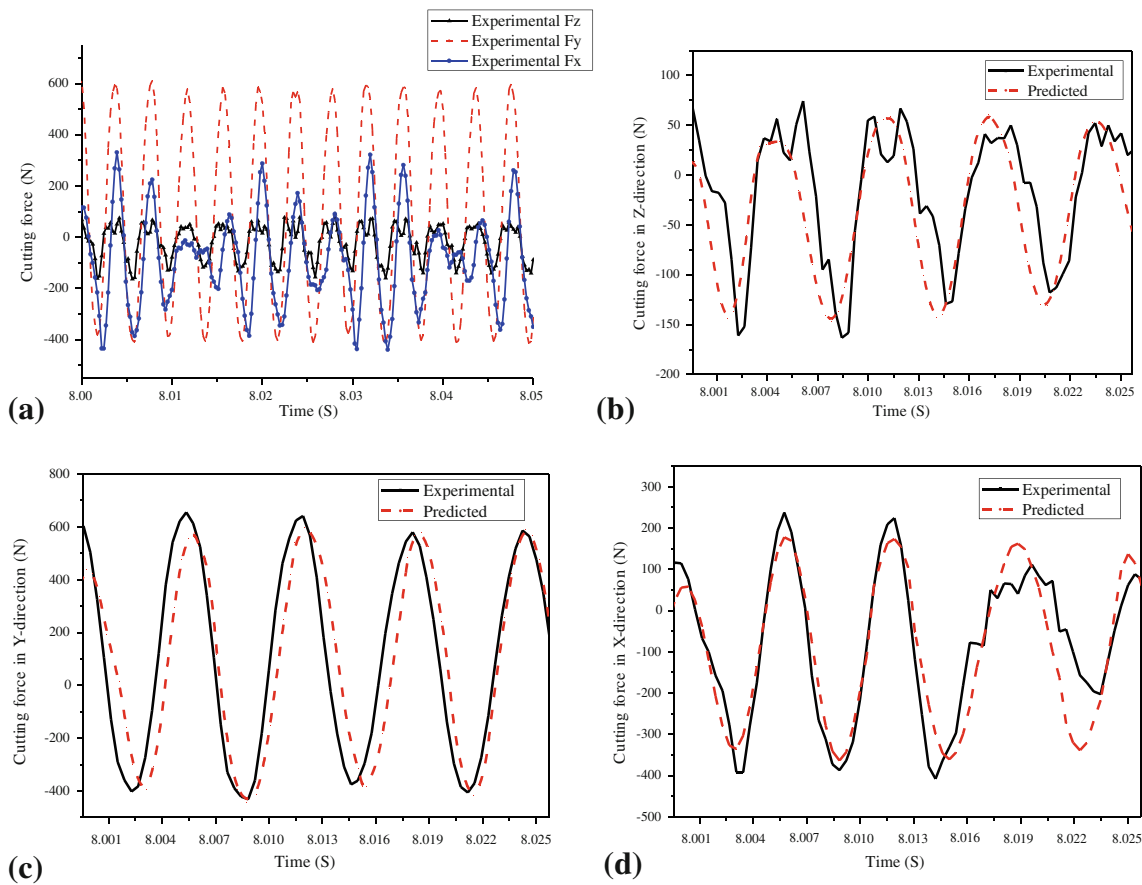


Fig. 8 Instantaneous UCT at feed rate a 0.05 mm/tooth, b 0.1 mm/tooth, and c 0.15 mm/tooth

obtained by Matlab integration using MATLAB mathematic tool, and then the cutting force of the whole milling cutter can be obtained by superposition according to the order of fixed phase difference, as shown follows:



**Fig. 9** Experimental and predicted cutting force of test 2: **a** experimental cutting force, **b** cutting force in Z-direction, **c** cutting force in Y-direction, and **d** cutting force in X-direction

$$\begin{aligned}
 F_x &= \sum_{j=1}^z F_{xj}(\theta_j) \\
 F_y &= \sum_{j=1}^z F_{yj}(\theta_j) \\
 F_z &= \sum_{j=1}^z F_{zj}(\theta_j)
 \end{aligned}
 \tag{7}$$

### 4 Cutting force prediction for fragment

In order to gain three-dimensional cutting forces  $F_x$ ,  $F_y$ , and  $F_z$  measured by the force measuring instrument in the coordinate system of the machine tool, cutting forces  $dF_{aj}$ ,  $dF_{rj}$ , and  $dF_{ij}$  predictions for fragment should be fulfilled at first. Figure 4 depicts the schematic of 3D FE modeling for cutting edge fragment. As mentioned in the previous analysis, each fragment could be regarded as a typical 3D oblique cutting model with the discretization of cutting edge involved in cutting process. Thereby, the 3D FE model for each fragment along the axis could be acquired. For the 3D FE analysis model, it is still necessary to determine the rake angle, the clearance angle, the cutting edge radius, the inclination angle, and the undeformed

chip thickness. Since the rake and the clearance angle in the 3D FE model are the namely normal and clearance angle, and the cutting edge radius is 0.03 mm, only the undeformed chip thickness should be estimated, which resolves the accuracy and efficiency of the FE simulation.

The undeformed chip thickness in the milling process is the envelope area of the movement track of adjacent cutter teeth, as shown in Fig. 3. In order to facilitate the FE simulation, as well as reflect the cutting force changing in the milling process as the uncut chip thickness decreases from the maximum  $h_{max}$  to 0 during the run-in and run-out process of single cutter tooth, the equal volume treatment method is adopted according to the energy conservation. Namely, under the condition that the axial cutting depth of the fragment  $da_p$  is constant, the cutting area in the  $XOY$  plane is guaranteed to be constant. The maximum uncut chip thickness  $h_{max}$  for the cutting-in process of cutter tooth in the down milling process can be expressed as

$$h_{max} = \left[ f_z \cdot \left\{ \frac{D/a_e - 1}{(D/2a_e)^2 (1 - v_f/V_c)^2 - v_f \cdot D/V_c \cdot a_e} \right\}^{1/2} \right] \cdot \cos i
 \tag{8}$$



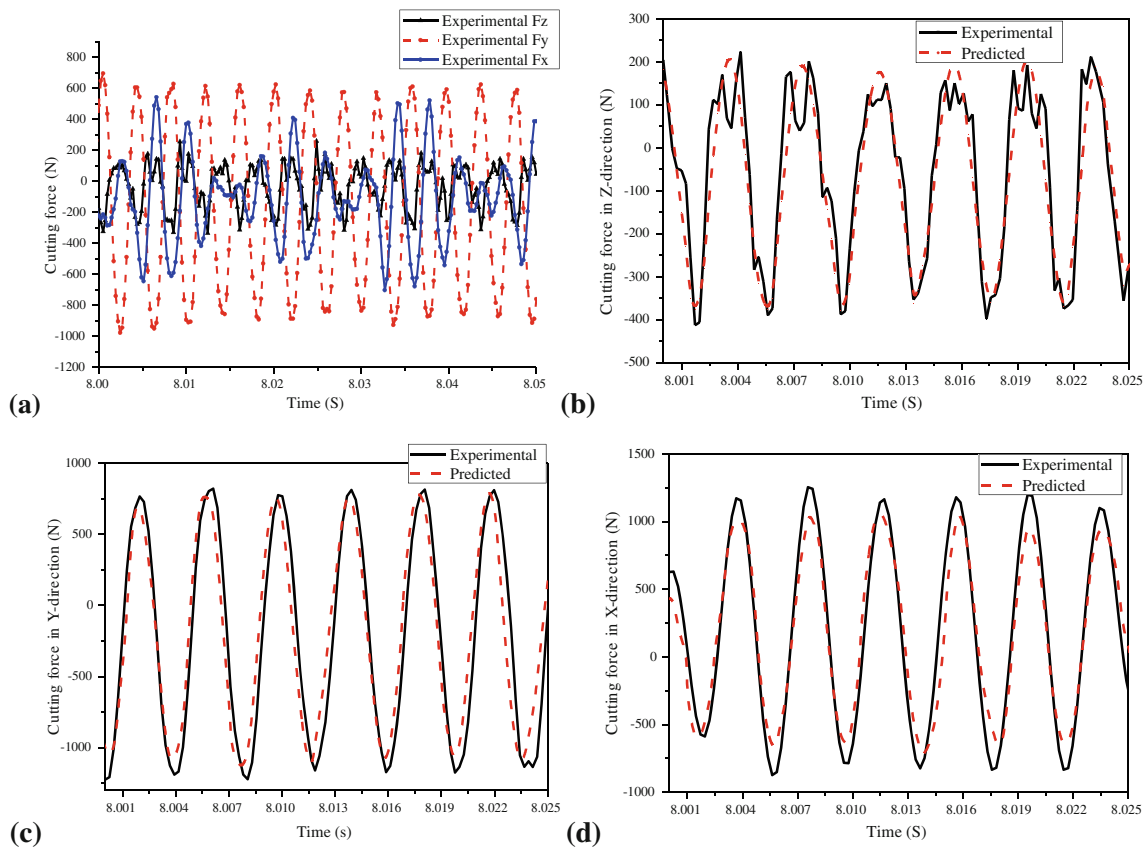


**Fig. 10** Experimental and predicted cutting force of test 5: **a** experimental cutting force, **b** cutting force in Z-direction, **c** cutting force in Y-direction, and **d** cutting force in X-direction

where  $f_z$  is the feed per tooth,  $D$  is the diameter of the milling cutter,  $\alpha_e$  is the radial cutting depth,  $v_c$  is the cutting speed,  $v_f$  is the feed speed, and  $i$  is the tool cutting edge inclination angle.

The undeformed chip length can be expressed as follow:

$$l = \frac{\alpha_e D}{2} - \frac{a_e v_f}{v_c} \left( \frac{D}{a_e} - 1 \right)^{1/2} \quad (9)$$

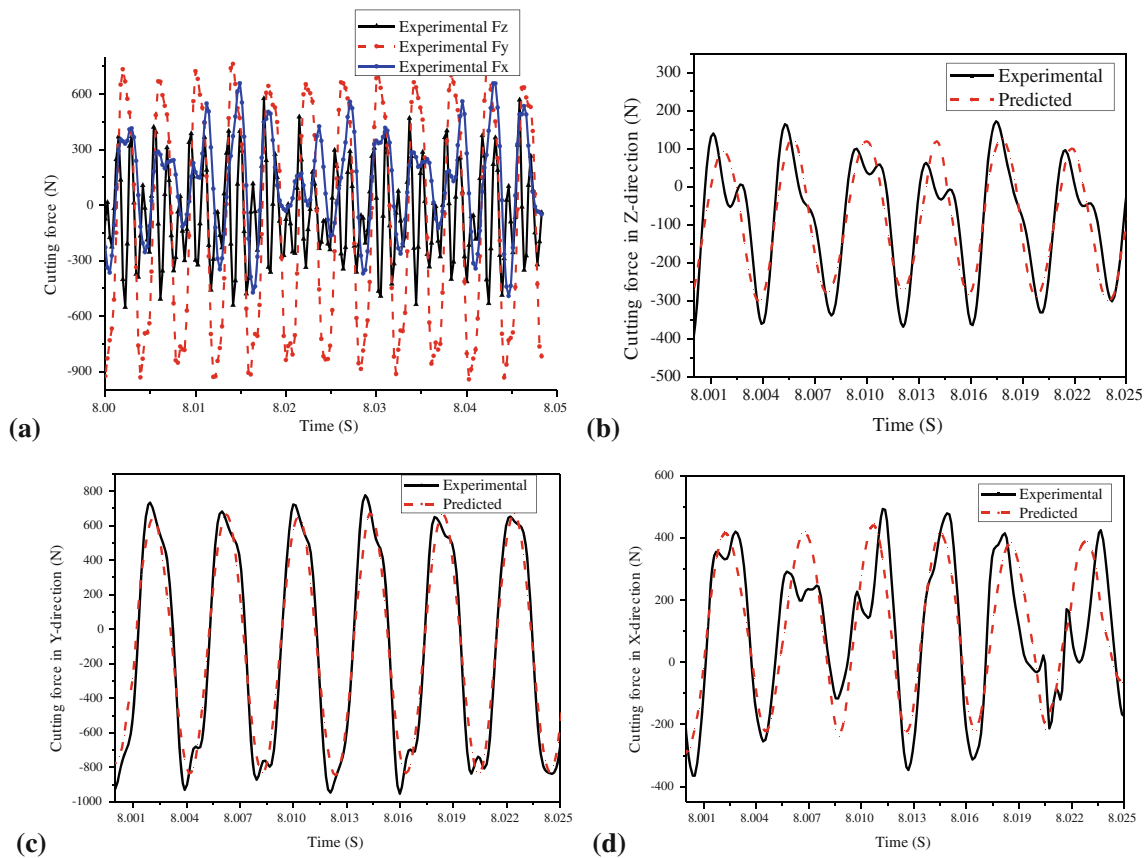
Based the above analysis, the maximum undeformed chip thickness as the run-in moment of fragment edge was set as  $h_{max}$  in the 3D FE model and the equivalent undeformed chip length could be obtained by the area method based on energy conservation. So far, all geometric boundary conditions of the 3D FE model have been defined.

Table 1 shows the parameters of the cutting edge fragment in 3D FE model. According to Table 1, it can be conducted that the run-in and run-out relationship of the cutting edge could be determined with Eq. (6). By using of mathematic tool MATLAB, data sampling for  $\theta_j$  can be performed with a certain increment within the range of  $[\theta_{min}, \theta_{max} + \psi]$ . Besides,  $x_{down}$  and  $x_{up}$  of the position angle  $\theta_j$  could be determined by Eq. (6); as a result, the instantaneous cutting force of

a single cutting edge corresponding to the position angle could be obtained by Eq. (7).

Simulations were performed with Third Wave Systems *AdvantEdge* finite element-based modeling software, which integrates advanced finite element numerics and material modeling for customize for machining applications. An explicit dynamic, thermo-mechanically coupled finite element modeling with Lagrangian method was applied to predict cutting force in flank milling of Inconel 718. The element topology used is a six-noded quadratic triangle element with three corner and three midsize nodes. Continuous adaptive remeshing is used to correct the problem of element distortion due to high deformations. The larger elements are refined and smaller elements coarsened at regular intervals.

The  $J-C$  material model was utilized, wherein the flow stress was dependent on the strain, strain rate, and temperature. This model is suitable for modeling cases with high strain, high strain rate, high strain hardening, and nonlinear material properties, which represents the main numerical challenges of metal cutting modeling. Additionally, it has been widely used in modeling cutting processes and has proven its suitability [26]. The following  $JC$  equation was utilized:



**Fig. 11** Experimental and predicted cutting force of test 8: **a** experimental cutting force, **b** cutting force in Z-direction, **c** cutting force in Y-direction, and **d** cutting force in X-direction

$$\sigma = \left[ A + B \left( \frac{\varepsilon^{pl}}{\varepsilon_0} \right)^n \right] \left[ 1 + C \ln \left( \frac{\varepsilon^{pl}}{\varepsilon_0} \right) \right] (1 - \hat{\theta}^m) \quad (10)$$

where  $n$  is the strain hardening index,  $A$ – $C$  and  $m$  are the material parameters, and  $\hat{\theta}$  is the nondimensional temperature given by

$$\hat{\theta} = \begin{cases} 0 & \text{for } \theta < \theta_t \\ \frac{\theta - \theta_t}{\theta_m - \theta_t} & \text{for } \theta_t \leq \theta \leq \theta_m \\ 1 & \text{for } \theta > \theta_m \end{cases} \quad (11)$$

where  $\theta$  is the current temperature,  $\theta_m$  is the melting temperature, and  $\theta_t$  is the transition temperature, below which temperature dependence does not exist.

The physical properties of the workpiece and the  $J$ – $C$  parameters for Inconel 718 alloy are given in Tables 2 and 3, respectively. Further,  $JC$  failure model is adopted, as shown follow:

$$\bar{\varepsilon}^{fpl} = [D_1 + D_2 \exp(D_3 \sigma)] [1 + D_4 \ln \varepsilon] [1 + D_5 \ln T] \quad (12)$$

where,  $\sigma$ ,  $\varepsilon$ , and  $T$  are the stress, strain rate, and temperature, respectively, and  $D_1$ ,  $D_2$ ,  $D_3$ ,  $D_4$ , and  $D_5$  are material-

dependent fracture constants.

Figure 5 presents the 3D FE simulated cutting process of cutting edge fragment; with the discretization of cutting edge, simulation time can be reduced dramatically compared with the 3D simulation of the entire end milling cutters. It could be found that the temperature in the cutting process is very high, as the maximum temperature reaches 1214.15 °C. As well as the high temperature, Mises stress in the cutting area reaches to 1000 MPa.

### 5 Experimental procedure

In order to validate cutting force model, milling tests were carried out on DMU70V five-axis CNC machining center with dry cutting, as shown in Fig. 6. The milling tests were carried out under down milling with the using of BT40 tool holder. The milling cutter is a carbide end milling tools with cylindrical shank and 16 mm diameter, which has four cutting edges, 0.03 mm cutting edge radius, 0.2 mm corner radius and 30° helix angle, 8° normal rake angle, and 5° clearance angle. The workpiece material is Inconel 718; its chemical compositions are as shown in Table 4. KISTLER 9272 piezoelectric dynamometer, Kistler 5017B charge amplifier, and

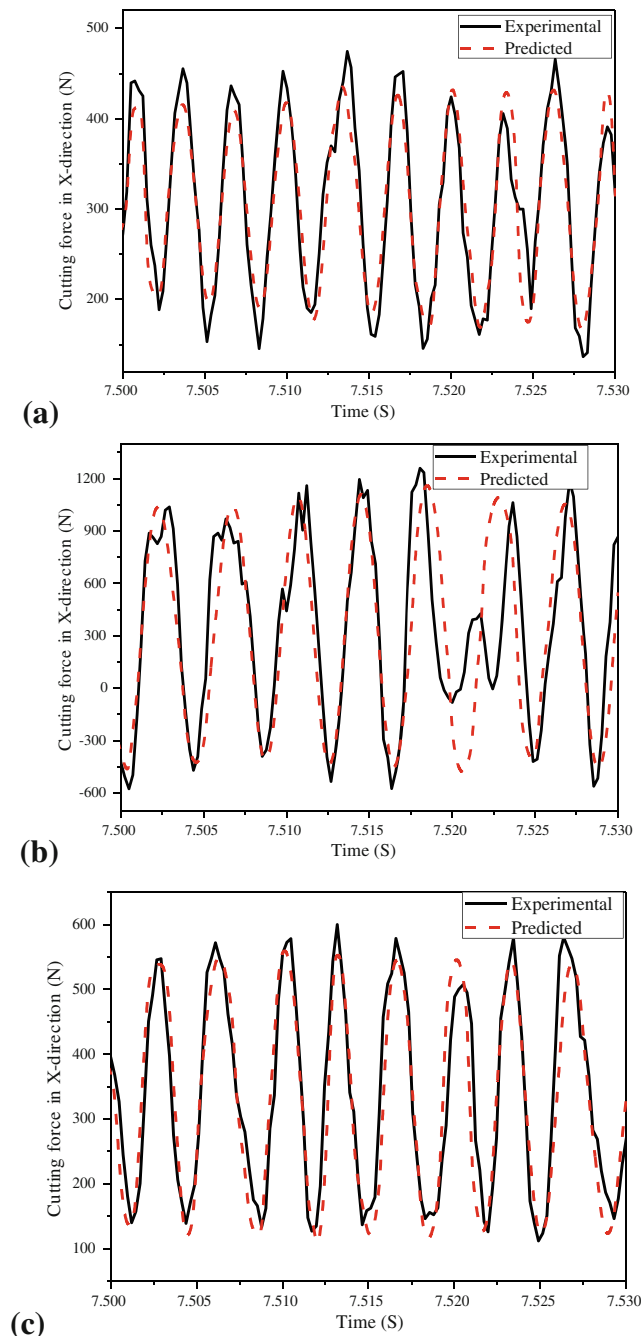


**Fig. 12** Experimental and predicted cutting force in Y-direction for Test 3 (a), 6 (b), and 9 (c)

corresponding data acquisition and processing system were used to measure the cutting force. The sensitivity of  $F_x$  and  $F_y$  is  $-7.8 \text{ pC/N}$ , the sensitivity of  $F_z$  is  $-3.5 \text{ pC/N}$ , the natural frequency of  $f_{nx}$  and  $f_{ny}$  is  $3.1 \text{ kHz}$ , and the natural frequency of  $f_{nz}$  is  $6.3 \text{ kHz}$ . The sampling frequency is  $4096 \text{ Hz}$ .

A milling tests was designed with the changing of cutting speed and feed per tooth, while the axis depth of cut and radial depth of cut is  $15 \text{ mm}$  and  $0.5 \text{ mm}$ , respectively, as shown in Table 5. Therefore, the effects of cutting speed and feed per tooth on cutting force could be

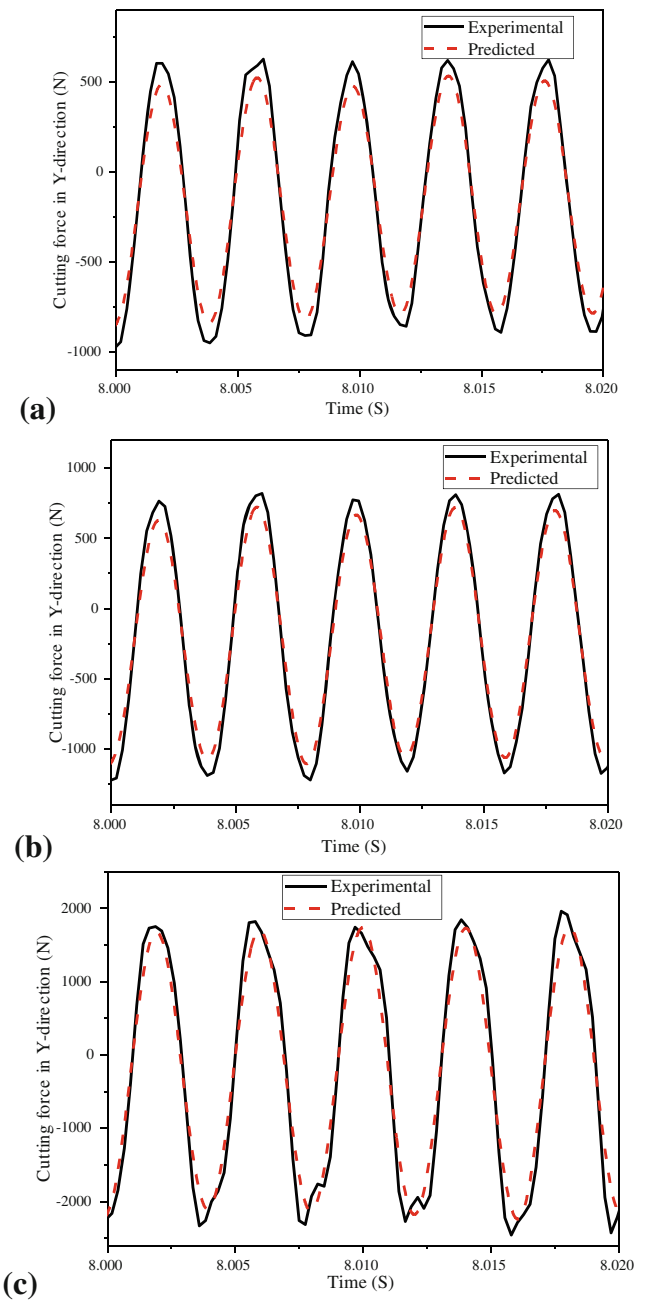


**Fig. 13** Experimental and predicted cutting force in Y-direction for Test 5 (a), 6 (b), and 7 (c)

investigated directly. Figure 7 shows the experimental cutting force for test 5.

## 6 Discussion

### 6.1 Experimental verification

Figure 8 shows the analysis of chip thickness with cutting angle. It is found that the chip thickness is theoretically reduced from the maximum value to 0, and then recycled. In

fact, through the model calculation, when the cutter cuts into the workpiece, the chip thickness does not immediately increase to the maximum value, but there is a lag, which is more consistent with the actual situation.

In order to validate the cutting force prediction model, a series of milling test were carried out and the comparison of predicted and experimental cutting force for test 2, test 5, and test 8, which represented the low, middle, and high cutting speed, respectively, were conducted in Figs. 9, 10, and 11. Results showed that the predicted cutting force coincided well with that of milling experiments, especially in  $X$ - and  $Y$ -directions. Due to interference and other factors in the actual milling test, the experimental measurement force in the  $Z$ -direction fluctuated at the peak position, while the simulation prediction force is more stable.

In sum, it is found that the average absolute error of the cutting force measured and predicted in the three directions is: 14.49% in the  $Z$ -direction, 7.73% in the  $Y$ -direction, and 9.68% in the  $X$ -direction. Except for the large fluctuations in the cutting force measured in the  $Z$ -direction due to experimental errors, the average absolute error of cutting force between experimental and predicted in the  $X$ - and  $Y$ -directions is within 10%; thus, the cutting force predicted by the model could be considered to be reliable.

## 6.2 Effect of cutting speed

Figure 12 presents the experimental and predicted cutting force for tests 3, 6, and 9, with cutting speeds of 30 m/min, 70 m/min, and 110 m/min, respectively. Results show that the predicted cutting forces are in good agreement with that of experimental. Cutting force increased as the cutting speed increased from 30 to 70 m/min. However, due to the thermal soften effect induced by high temperature and the reduction of deformation coefficient with the reduction of frictional coefficient, the cutting force decreased when the cutting speed continuously increased to 110 m/min. In contrast, the strain hardening effect gave rise to cutting force increasing when the cutting speed increased from 30 to 70 m/min. Similar results could be found in Yilmaz et al.'s work [29].

## 6.3 Effect of feed per tooth

The analysis of the influence of feed per tooth on cutting force is depicted in Fig. 13. The cutting force dramatically increased with the increasing of feed per tooth at the same cutting speed. Specially, the maximal cutting force in  $Y$ -direction increased from 1000 to 1500 N as the feed per tooth increased from 0.05mm/tooth to 0.1mm/tooth. When the feed per tooth increased to 0.15 mm/tooth, the cutting force in  $Y$ -direction increased to 2000 N, twice as much as that of 0.1 mm/tooth. In spite of high machining efficiency for high feed rate, it is

obvious that the increasing of feed per tooth results in remarkable increasing of cutting force.

## 7 Conclusions

The variation of the cutting force could greatly affect the stability and tool life of the milling cutter, as well as the machining precision and efficiency. The present work is thus aimed at developing a new cutting force model for flank milling, which eliminates the drawbacks of pure analytical force model, DBRM model and full 3D FE model. For this purpose, a hybrid approach for cutting force prediction in flank milling is proposed and a series of milling tests are carried out for the model validation. Based on the results acquired, the following conclusions can be drawn.

- (3) The hybrid cutting force model is conducted by discretizing cutting edge into fragments based on finite difference method and regarding each fragment as a 3D oblique cutting FEM model. With the integration of 3D predicted cutting force along the axis, the predicted cutting force can be obtained.
- (4) The predictive results show that the hybrid model predicts the cutting force  $F_x$  and  $F_y$ , with an average absolute error of 7.73% and 9.68%, while a higher prediction error of 14.49% is obtained for  $F_z$ . The overall force error is around 15%, and the predictions are in good agreement with the experimental data.
- (5) Both the experimental cutting force and predicted cutting force increase with the feed per tooth; however, the cutting force increases when cutting speed increases from 30 to 70 m/min and then decreases when cutting speed increases from 70 to 110 m/min, which might attributed to reduction of material strength by thermal soften under the extreme high cutting temperature.

**Funding information** This research is supported by Shanghai science and technology talent plan (18QB1401600).

## References

1. Fan YH, Hao ZP, Zheng ML, Sun FL, Yang SC (2013) Study of surface quality in machining nickel-based alloy Inconel 718. Int J Adv Manuf Technol 69(9-12):2659–2667
2. Wojciechowski S, Matuszak M, Powalka B, Madajewski M, Maruda RW, Krolczyk GM (2019) Prediction of cutting forces during micro end milling considering chip thickness accumulation. Int J Mach Tools Manuf 147:103466
3. Zhang T, Liu ZQ, Xu CH (2015) Theoretical modeling and experimental validation of specific cutting force for micro end milling. Int J Adv Manuf Technol 77:1433–1441

4. Srinivasa YV, Shunmugam MS (2013) Mechanistic model for prediction of cutting forces in micro end-milling and experimental comparison. *Int J Mach Tools Manuf* 67:18–27
5. Harry O-O, Patxi AO, Pedro JAA (2019) Analytical modeling of the uncut chip geometry to predict cutting forces in orthogonal centric turn-milling operations. *Int J Mach Tools Manuf* 144: 103428
6. Ma JW, Jia ZY, Wang FJ, Gao YY, Liu Z (2016) A new cutting force modeling method in high-speed milling of curved surface with difficult-to-machine material. *Int J Adv Manuf Technol* 84: 2195–2205
7. Wan M, Lu MS, Zhang WH, Yang Y (2012) A new ternary-mechanism model for the prediction of cutting forces in flat end milling. *Int J Mach Tools Manuf* 57:34–45
8. Wei ZC, Li SQ, Guo ML, Wang J, Liu SX (2019) Plane surface milling force prediction with fillet end milling cutter under pre-determined inclination angle. *Int J Adv Manuf Technol* 103: 2849–2864
9. Wang SB, Geng L, Zhang YF, Liu K, Ng TE (2015) Cutting force prediction for five-axis ball-end milling considering cutter vibrations and run-out. *Int J Mech Sci* 96-97:206–215
10. Guo ML, Wei ZC, Wang MJ, Li SQ, Liu SX (2018) An identification model of cutting force coefficients for five-axis ball-end milling. *Int J Adv Manuf Technol* 99:937–949
11. Berglind L, Plakhotnik D, Ozturk E (2017) Discrete cutting force model for 5-axis milling with arbitrary engagement and feed direction. 16<sup>th</sup> CIRP Conference on Modelling of Machining Operations 58: 445–450
12. Su X, Wang G, Yu JC, Jiang F, Li JF, Rong YM (2016) Predictive model of milling force for complex profile milling. *Int J Adv Manuf Technol* 87:1653–1662
13. Tuysuz O, Altintas Y, Feng H-Y (2013) Prediction of cutting forces in three and five-axis ball-end milling with tool indentation effect. *Int J Mach Tools Manuf* 66:66–81
14. Wojciechowski S, Mrozek K (2017) Mechanical and technological aspects of micro ball end milling with various tool inclinations. *Int J Mech Sci* 134:424–435
15. Thellaputta GR, Raju CS, Bose PSC, Rao CSP (2018) Adaptive neuro fuzzy model development for prediction of cutting forces in milling with rotary tools. *Mater Today Proc* 5:7429–7436
16. Zhang XW, Yu TB, Zhao J (2020) An analytical approach on stochastic model for cutting force prediction in milling ceramic matrix composites. *Int J Mech Sci* 168:105314
17. Aritimuno P, Lazcano X, Sela A, Basagoiti R, Arrazola PJ (2018) An optimization methodology for material databases to improve cutting force predictions when milling martensitic stainless steel JETHETE-M152. 8<sup>th</sup> CIRP Conference on High Performance Cutting 77: 287-290
18. Jamal S-A, He YL, Qin L (2019) Cutting force prediction in milling CFRPs with complex cutter geometries. *J Manuf Process* 45:720–731
19. Sahoo P, Pratap T, Patra K (2019) A hybrid modelling approach towards prediction of cutting forces in micro end milling of Ti-6Al-4V titanium alloy. *Int J Mech Sci* 150:495–509
20. Cai SJ, Yao B, Feng W, Cai ZQ (2019) An improved cutting force prediction model in the milling process with a multi-blade face milling cutter based on FEM and NURBS. *Int J Adv Manuf Technol* 104:2487–2499
21. Kiran K, Kayacan MC (2019) Cutting force modeling and accurate measurement in milling of flexible workpieces. *Mech Syst Signal Process* 133:106284
22. Ducobu F, Rivière-Lorphèvre E, Filippi E (2017) Finite element modelling of 3D orthogonal cutting experimental tests with the Coupled Eulerian-Lagrangian (CEL) formulation. *Finite Elem Anal Des* 134:27–40
23. Nasr MNA, Ammar MMA (2017) An evaluation of different damage models when simulating the cutting process using FEM. *CIRP* 58:134–139
24. Pratap T, Patra K, Dyakonov AA (2015) Modelling cutting force in micro-milling of Ti-6Al-4V titanium alloy. *Procedia Eng* 129:134–139
25. Jing XB, Li HZ, Wang J, Tian YL (2014) Modelling the cutting forces in micro-end-milling using a hybrid approach. *Int J Adv Manuf Technol* 7:9–12
26. Johnson GK, Cook WH (1983) A constitutive model and data for metals subjected to large strains large strain rates and high temperatures. In *The 7th International Symposium on Ballistics*, Hague, Netherlands
27. Lorentzon J, Jarvstrat N, Josefson BL (2009) Modelling chip formation of alloy 718. *J Mater Process Technol* 209:4645–4653
28. Haglund AJ, Kishawy HA, Rogers RJ (2008) An exploration of friction models for the chip-tool interface using an arbitrary Lagrangian-Eulerian finite element model. *Wear* 265:452–460
29. Bahattin YI, Ener K, Abdulkadir G (2018) Performance analysis of new external chip breaker for efficient machining of Inconel 718 and optimization of the cutting parameters. *J Manuf Process* 32: 553–563

**Publisher's note** Springer Nature remains neutral with regard to jurisdictional claims in published maps and institutional affiliations.